

Electronic Supplementary Information

for

Monomethylaluminum and dimethylaluminum pyrrolyaldiminates for the ring-opening polymerization of *rac*-lactide: Effects of ligand structure and coordination geometry

Sittichoke Thabthong,^a Tanin Nanok,^a Palangpon Kongsaree,^b Samran Prabpai,^b
and Pimpa Hormnirun^{*a}

^aDepartment of Chemistry, Faculty of Science, Kasetsart University, Bangkok 10900, Thailand

^bDepartment of Chemistry and Center for Excellence in Protein Structure and Function,
Faculty of Science, Mahidol University, Bangkok 10400, Thailand

*Corresponding author: fscipph@ku.ac.th

Table S1 Crystallographic data and structure refinement details for complex **3b**.

Chemical formula	C ₂₅ H ₂₅ AlN ₄
Formula weight (M)	408.49
Temperature (K)	298(2)
Dimension (mm)	0.30 × 0.20 × 0.15
Crystal system	orthorhombic
Space group	P2 ₁ 2 ₁ 2 ₁
<i>a</i> (Å)	9.9362(3)
<i>b</i> (Å)	12.7413(4)
<i>c</i> (Å)	<i>c</i> = 18.0469(11)
<i>α</i> (deg)	90
<i>β</i> (deg)	90
<i>γ</i> (deg)	90
<i>V</i> (Å ³)	2284.7(1)
<i>Z</i>	4
Calculated density (g/cm ³)	1.188
Reflections collected/unique	20688/4172
Number of observations [<i>I</i> > 2σ(<i>I</i>)]	2922
Final R indices [<i>I</i> > 2σ (<i>I</i>)]	R ₁ = 0.0460, wR ₂ = 0.1284

Table S2 Bond lengths (Å) and bond angles (°)

Bond lengths (Å)					
A11-N1	1.912(2)	N7-C8	1.422(4)	C29-H29A	0.959(3)
A11-N15	1.908(2)	C5-C6	1.406(4)	C29-H29B	0.959(3)
A11-N21	2.125(2)	C5-C4	1.386(4)	C29-H29C	0.960(3)
A11-N7	2.162(2)	C6-H6	0.960(3)	C25-C24	1.372(4)
A11-C29	1.963(3)	C20-H20	0.960(3)	C25-C26	1.365(5)
N1-C5	1.382(3)	C20-C19	1.408(4)	C25-C28	1.517(5)
N1-C2	1.360(3)	C16-H16	0.959(3)	C4-H4	0.960(3)
N15-C16	1.364(4)	C16-C17	1.373(5)	C4-C3	1.374(4)
N15-C19	1.378(4)	C2-H2	0.960(3)	C24-H24	0.960(3)
N21-C20	1.297(4)	C2-C3	1.370(4)	C3-H3	0.960(3)
N15-C16	1.364(4)	C22-C23	1.365(4)	C26-H26	0.960(3)
N15-C19	1.378(4)	C22-C27	1.377(4)	C26-C27	1.380(5)
N21-C20	1.297(4)	C19-18	1.365(5)	C18-H18	0.961(4)
N21-C22	1.429(3)	C23-H23	0.960(3)	C18-C17	1.375(5)
N7-C6	1.299(3)	C23-C24	1.377(4)	C8-C9	1.385(5)
C8-C13	1.393(5)	C13-C12	1.396(5)	C10-H10	0.961(4)
C17-H17	0.961(4)	C28-28A	0.960(4)	C10-C11	1.355(7)
C9-H9	0.960(4)	C28-28B	0.960(4)	C11-C14	1.531(5)
C9-C10	1.383(5)	C28-28C	0.959(4)	C14-H14A	0.959(5)
C27-H27	0.959(3)	C12-H12	0.960(5)	C14-H14B	0.960(6)
C13-H13	0.960(4)	C12-C11	1.378(6)	C14-H14C	0.961(5)
Bond angles (°)					
N1-A11-N15	115.47(9)	N21-C20-C19	118.2(2)	C23-C24-C25	121.8(3)
N1-A11-N21	90.74(8)	H20-C20-C19	121.1(3)	C23-C24-H24	120.5(3)
N1-A11-N7	80.23(8)	N15-C16-H16	119.6(3)	C25-C24-H24	117.7(3)
N1-A11-C29	125.3(1)	N15-C16-C17	110.1(3)	C2-C3-C4	107.3(2)
N15-A11-N21	81.38(9)	H16-C16-C17	130.3(3)	C2-C3-H3	120.0(3)
N15-A11-N7	91.13(9)	N1-C2-H2	118.8(2)	C4-C3-H3	132.7(3)
N15-A11-C29	119.3(1)	N1-C2-C3	110.8(2)	C25-C26-H26	119.6(3)
N21-A11-N7	164.53(9)	H2-C2-C3	130.4(3)	C25-C26-C27	122.6(3)
N21-A11-C29	97.9(1)	N21-C22-C23	122.1(2)	H26-C26-C27	117.8(3)
N7-A11-C29	97.5(1)	N21-C22-C27	119.7(2)	C19-C18-H18	120.2(3)
A11-N1-C5	115.9(2)	C23-C22-C27	118.2(3)	C19-C18-C17	107.4(3)
A11-N1-C2	138.3(2)	N15-C19-C20	116.3(2)	H18-C18-C17	132.4(4)
C5-N1-C2	105.5(2)	N15-C19-C18	109.8(3)	N7-C8-C9	121.4(3)
A11-N15-C16	139.8(2)	C20-C19-C18	133.8(3)	N7-C8-C13	120.4(3)
A11-N15-C19	114.5(2)	C22-C23-H23	119.6(3)	C9-C8-C13	118.2(3)
C16-N15-C19	105.7(2)	C22-C23-C24	120.9(3)	C16-C17-C18	107.0(3)
A11-N21-C20	109.5(2)	H23-C23-C24	119.5(3)	C16-C17-H17	120.8(3)
A11-N21-C22	131.2(2)	A11-C29-H29A	108.9(2)	C18-C17-H17	132.2(4)
C20-N21-C22	119.3(2)	A11-C29-H29B	109.4(2)	C8-C9-H9	119.2(3)
A11-N7-C6	109.2(2)	A11-C29-H29C	110.1(2)	C8-C9-C10	120.6(3)
A11-N7-C8	132.2(2)	H29A-C29-H29B	109.5(3)	H9-C9-C10	120.2(4)
C6-N7-C8	118.4(2)	H29A-C29-H29C	109.5(3)	C22-C27-C26	119.9(3)
N1-C5-C6	115.8(2)	H29B-C29-H29C	109.4(3)	C22-C27-H27	119.9(3)
N1-C5-C4	109.6(2)	C24-C25-C26	116.6(3)	C26-C27-H27	120.2(3)
C6-C5-C4	134.7(3)	C24-C25-C28	120.8(3)	C8-C13-H13	119.2(3)
N7-C6-C5	118.6(2)	C26-C25-C28	122.7(3)	C8-C13-C12	119.6(3)
N7-C6-H6	119.3(3)	C5-C4-H4	119.4(3)	H13-C13-C12	121.2(4)
C5-C6-H6	122.1(3)	C5-C4-C3	106.8(2)	C25-C28-H28A	110.1(3)
N21-C20-H20	120.7(3)	H4-C4-C3	133.7(3)	C25-C28-H28B	110.6(3)
C25-C28-H28C	107.6(3)	C13-C12-H12	119.1(4)	C9-C10-C11	121.9(4)
H28A-C28-H28B	109.5(4)	C13-C12-C11	121.5(4)	H10-C10-C11	117.5(4)
H28A-C28-H28C	109.5(4)	H12-C12-C11	119.3(4)	C12-C11-C10	118.2(4)
H28B-C28-H28C	109.5(4)	C9-C10-H10	120.6(4)	C12-C11-C14	119.2(4)

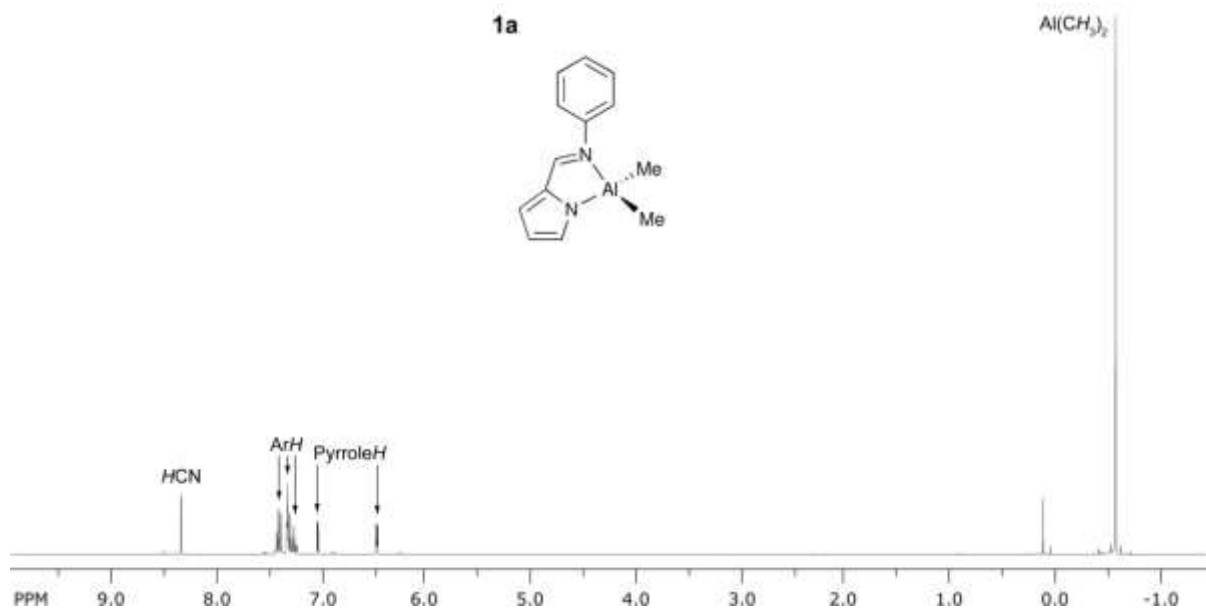


Fig. S1 400 MHz ¹H NMR spectrum of complex **1a** in CDCl₃.

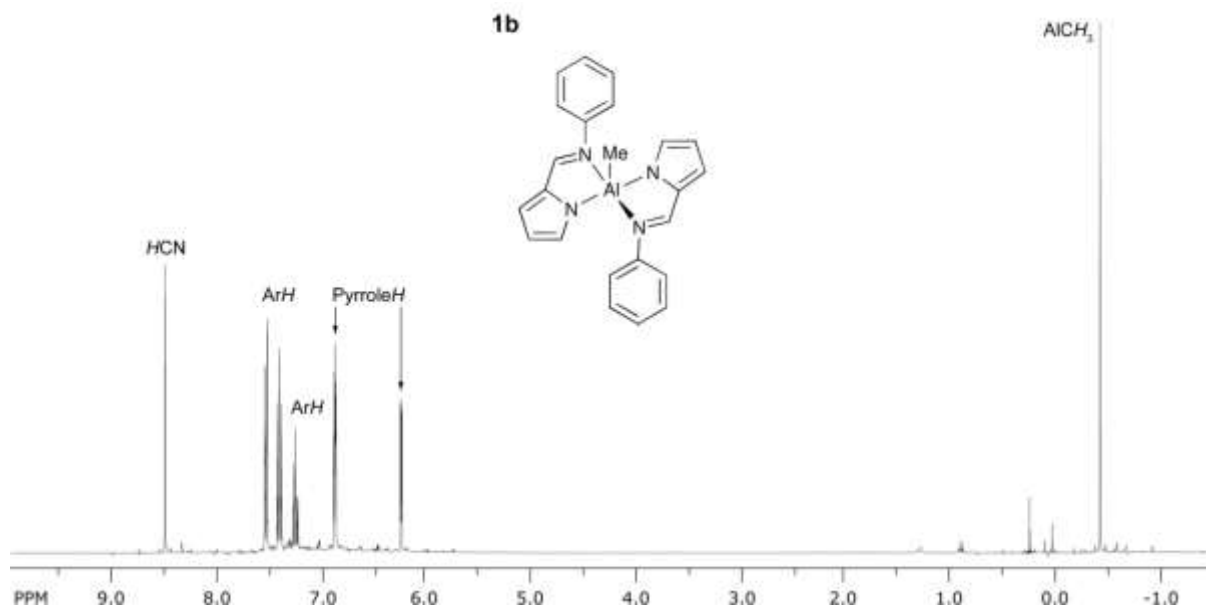


Fig. S2 400 MHz ¹H NMR spectrum of complex **1b** in CDCl₃.

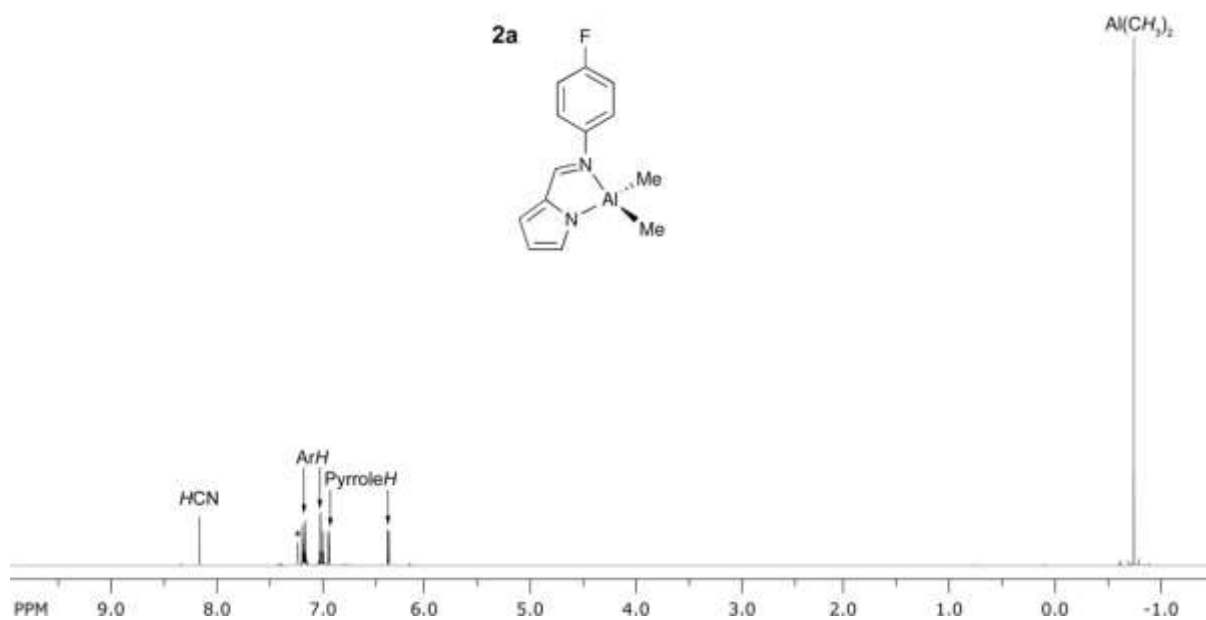


Fig. S3 400 MHz ^1H NMR spectrum of complex **2a** in CDCl_3 (* = residual CHCl_3).

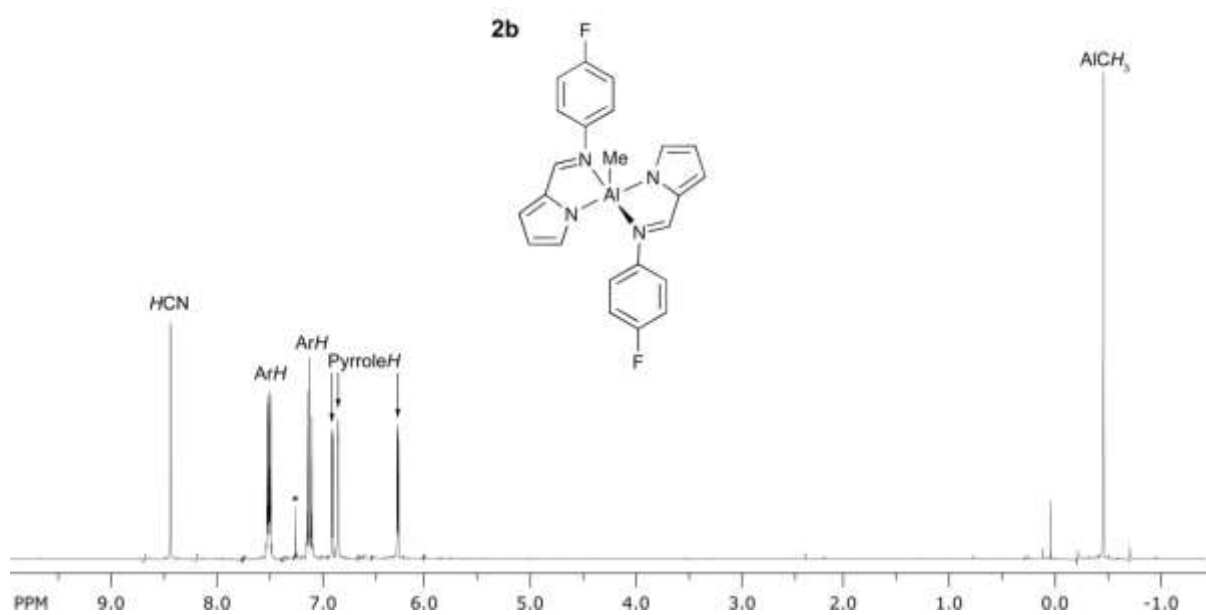


Fig. S4 400 MHz ^1H NMR spectrum of complex **2b** in CDCl_3 (* = residual CHCl_3).

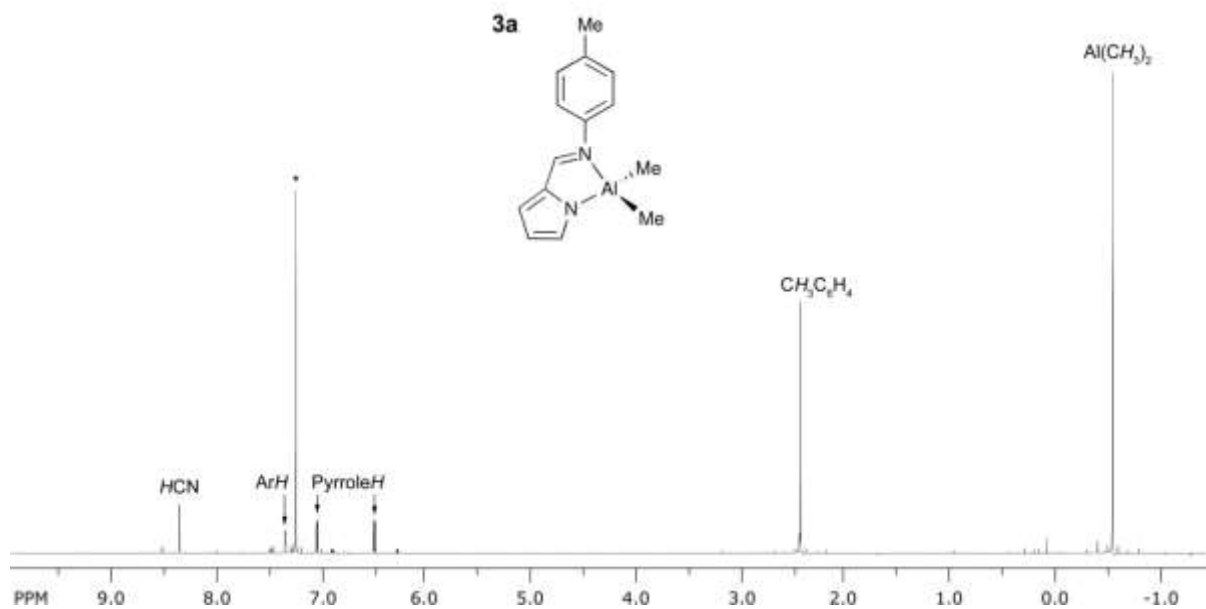


Fig. S5 400 MHz ¹H NMR spectrum of complex **3a** in CDCl₃ (* = residual CHCl₃).

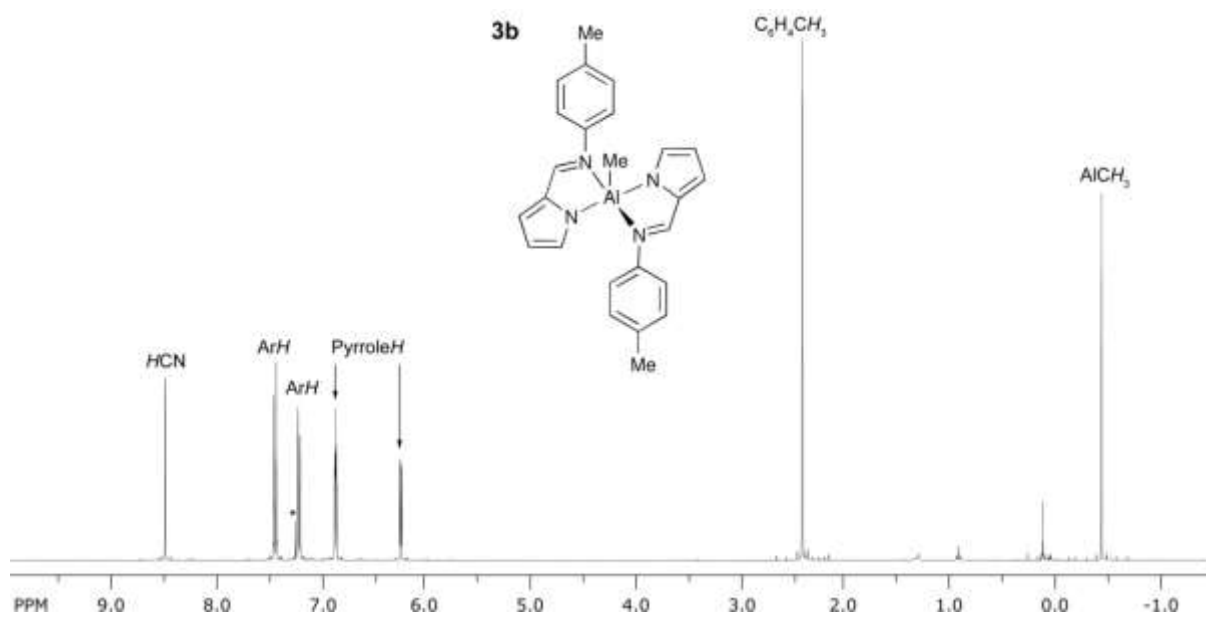


Fig. S6 400 MHz ¹H NMR spectrum of complex **3b** in CDCl₃ (* = residual CHCl₃).

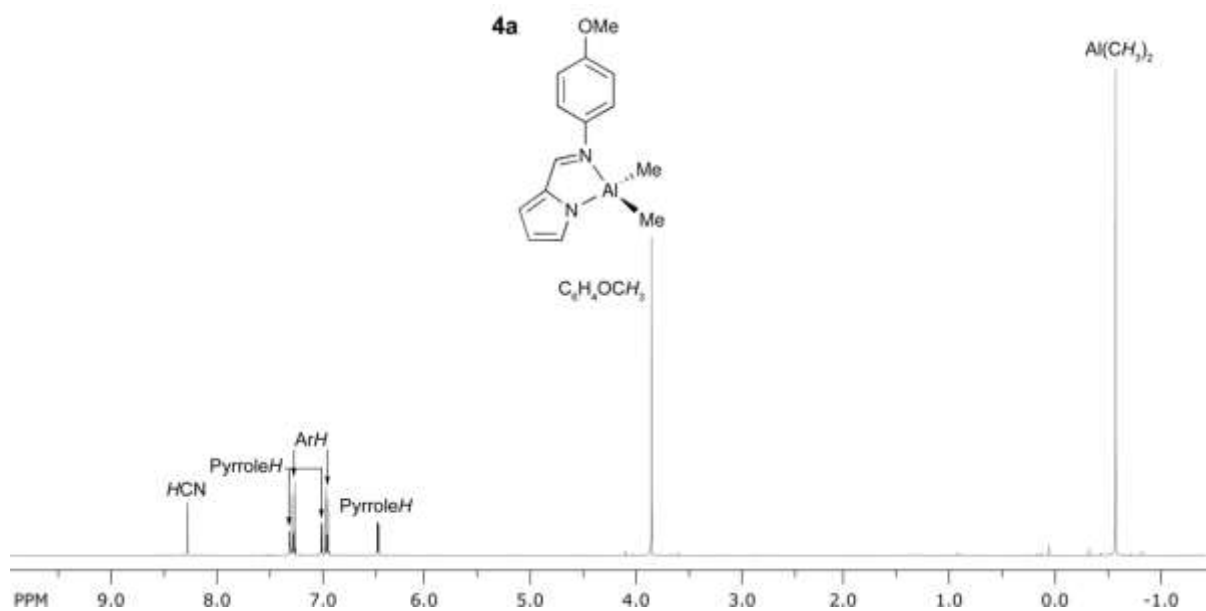


Fig. S7 400 MHz ¹H NMR spectrum of complex **4a** in CDCl₃.

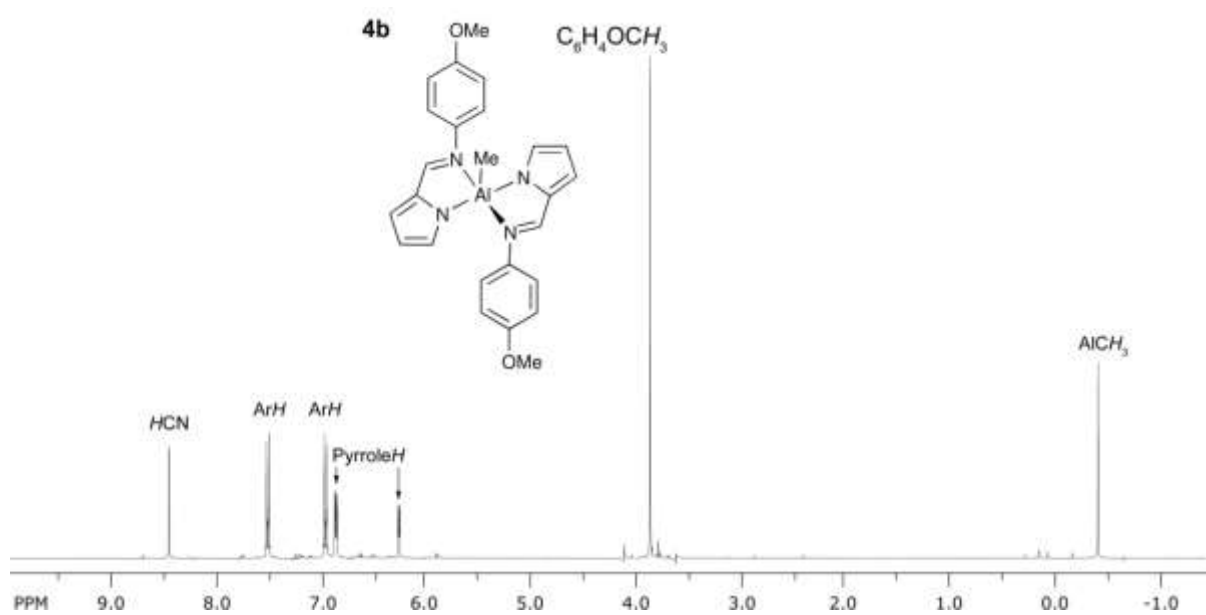


Fig. S8 400 MHz ¹H NMR spectrum of complex **4b** in CDCl₃.

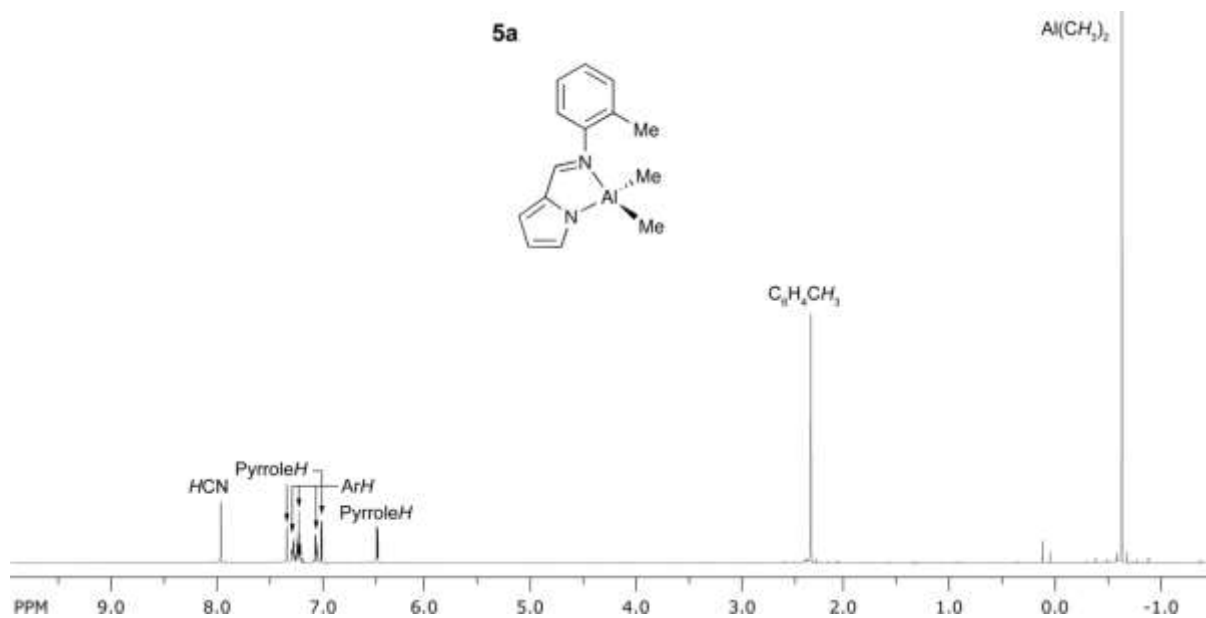


Fig. S9 400 MHz ¹H NMR spectrum of complex **5a** in CDCl₃.

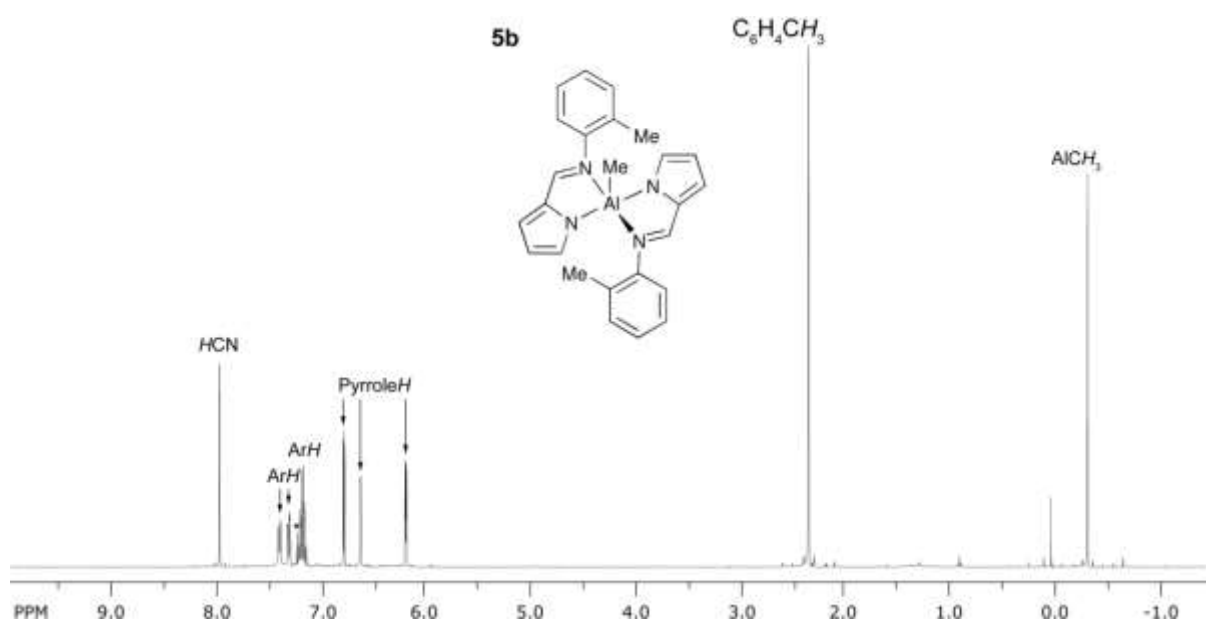


Fig. S10 400 MHz ¹H NMR spectrum of complex **5b** in CDCl₃ (* = residual CHCl₃).

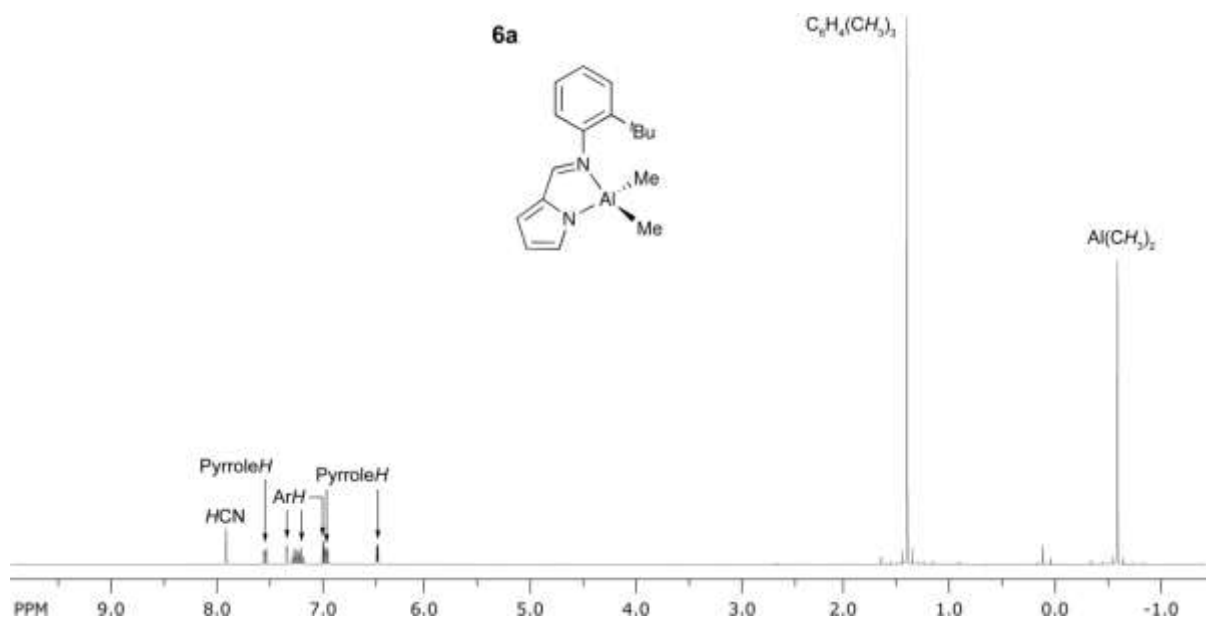


Fig. S11 400 MHz ¹H NMR spectrum of complex **6a** in CDCl₃.

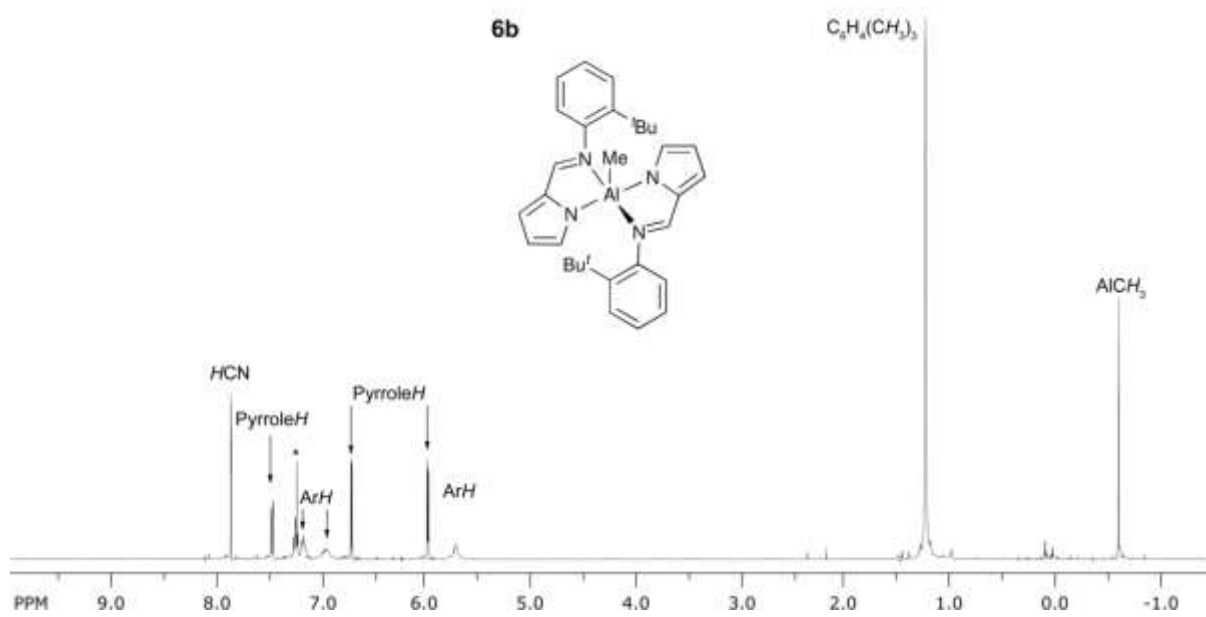


Fig. S12 400 MHz ¹H NMR spectrum of complex **6b** in CDCl₃.

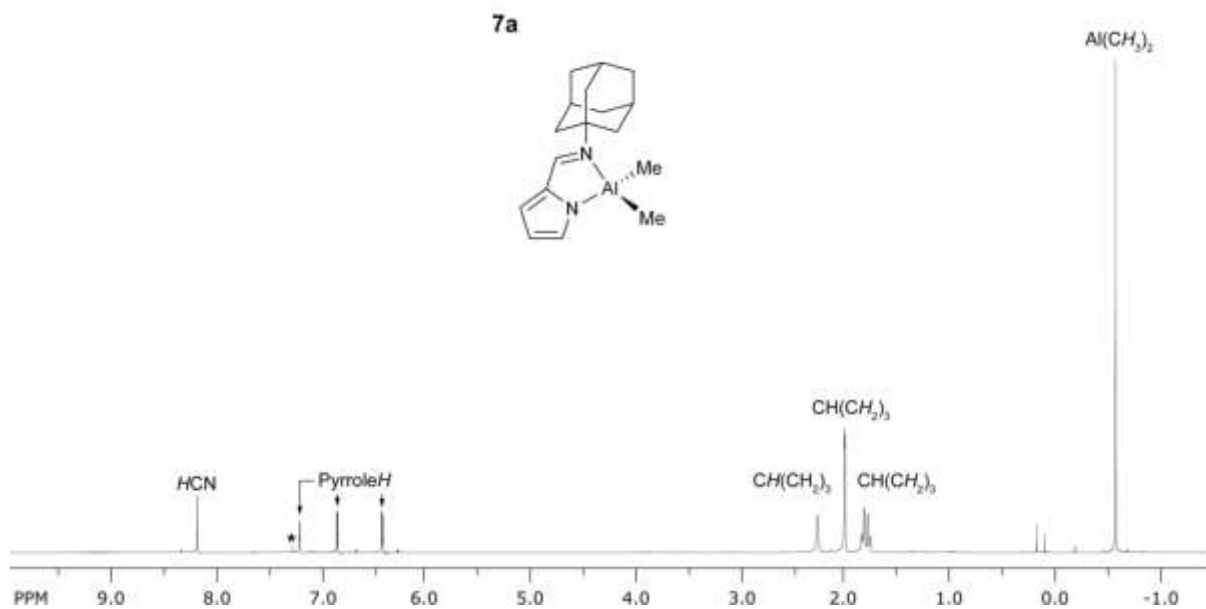


Fig. S13 400 MHz ¹H NMR spectrum of complex **7a** in CDCl₃ (* = residual CHCl₃).

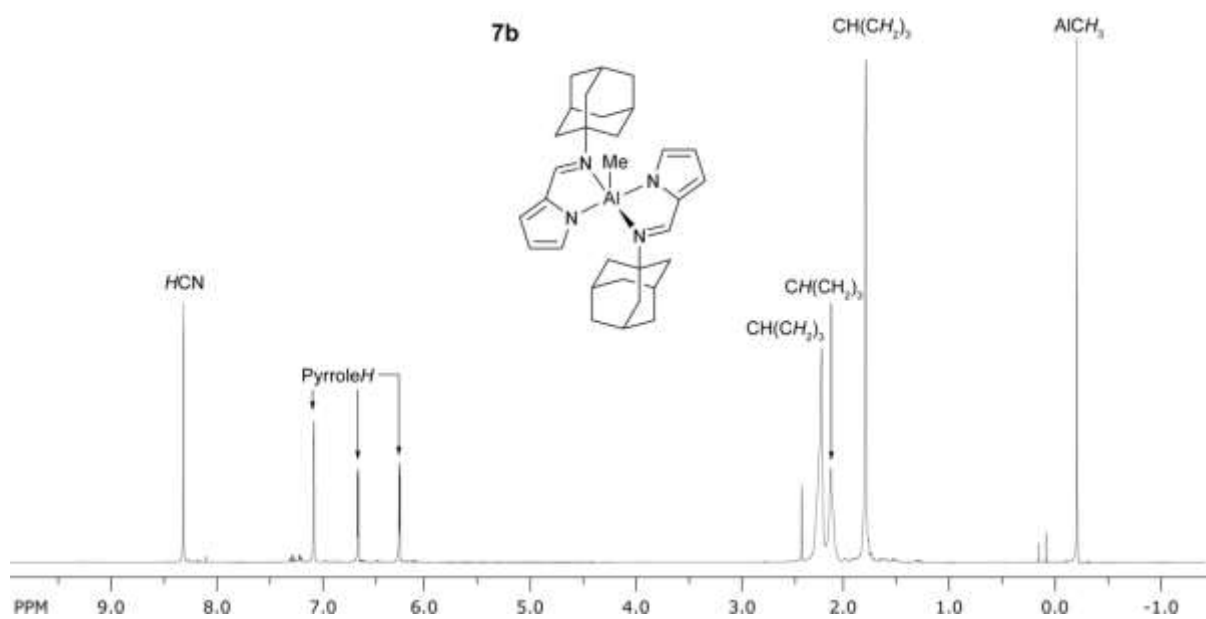


Fig. S14 400 MHz ¹H NMR spectrum of complex **7b** in CDCl₃.

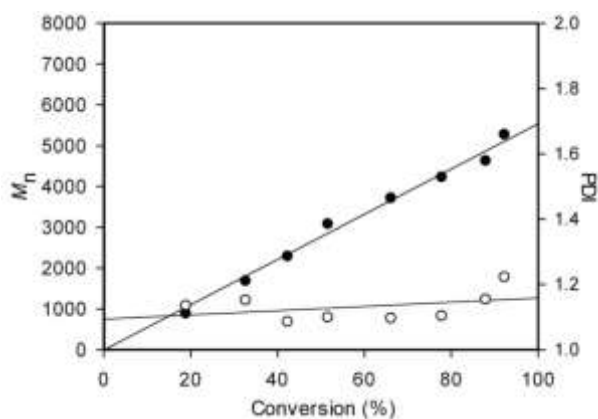


Fig. S15 Plots of PLA M_n (●) and PDI (○) as a function of monomer conversion for a *rac*-LA polymerization using **1b**/PhCH₂OH ([LA]₀/[Al] = 50, toluene, 70 °C)

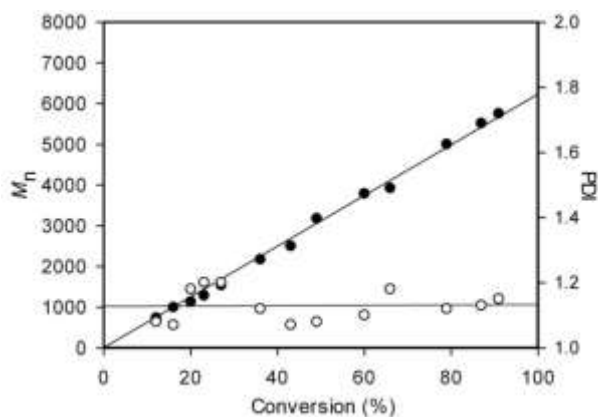


Fig. S16 Plots of PLA M_n (●) and PDI (○) as a function of monomer conversion for a *rac*-LA polymerization using **2a**/PhCH₂OH ([LA]₀/[Al] = 50, toluene, 70 °C)

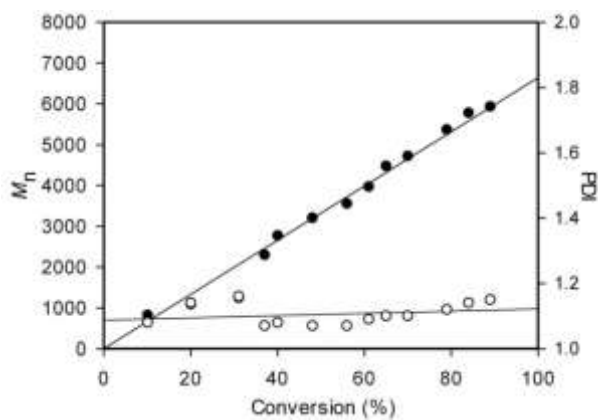


Fig. S17 Plots of PLA M_n (●) and PDI (○) as a function of monomer conversion for a *rac*-LA polymerization using **2b**/PhCH₂OH ([LA]₀/[Al] = 50, toluene, 70 °C)

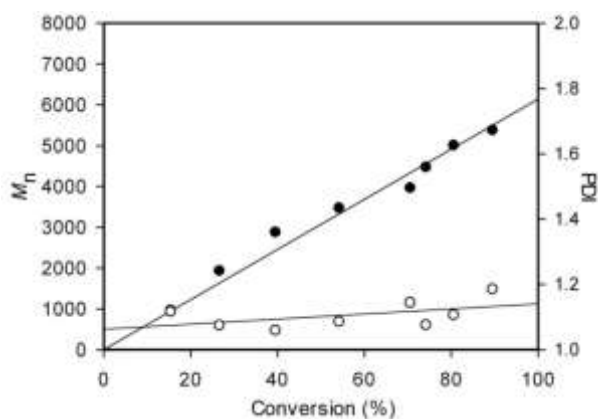


Fig. S18 Plots of PLA M_n (●) and PDI (○) as a function of monomer conversion for a *rac*-LA polymerization using **3a**/PhCH₂OH ([LA]₀/[Al] = 50, toluene, 70 °C)

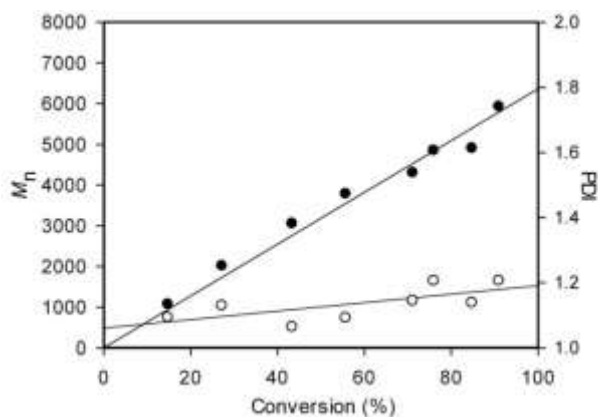


Fig. S19 Plots of PLA M_n (●) and PDI (○) as a function of monomer conversion for a *rac*-LA polymerization using **3b**/PhCH₂OH ([LA]₀/[Al] = 50, toluene, 70 °C)

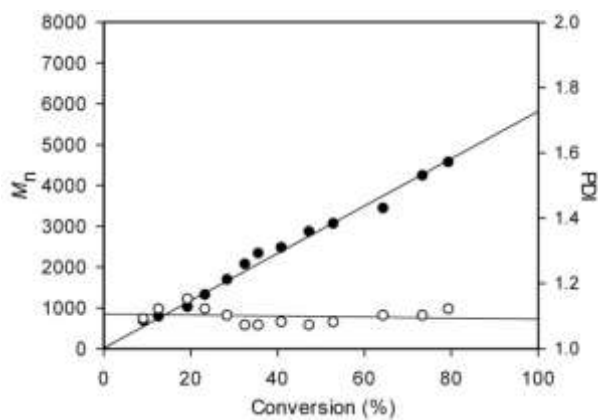


Fig. S20 Plots of PLA M_n (●) and PDI (○) as a function of monomer conversion for a *rac*-LA polymerization using **4a**/PhCH₂OH ([LA]₀/[Al] = 50, toluene, 70 °C)

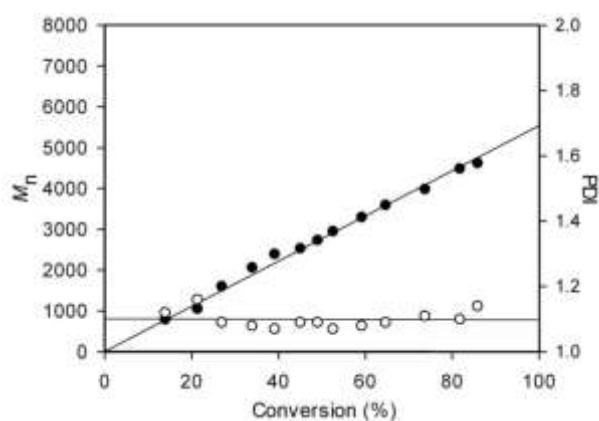


Fig. S21 Plots of PLA M_n (●) and PDI (○) as a function of monomer conversion for a *rac*-LA polymerization using **4b**/PhCH₂OH ([LA]₀/[Al] = 50, toluene, 70 °C)

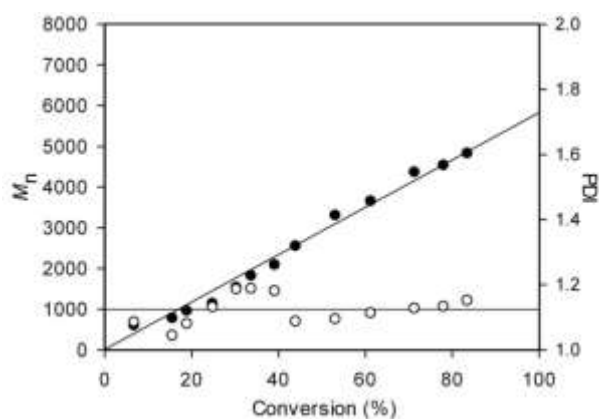


Fig. S22 Plots of PLA M_n (●) and PDI (○) as a function of monomer conversion for a *rac*-LA polymerization using **5a**/PhCH₂OH ([LA]₀/[Al] = 50, toluene, 70 °C)

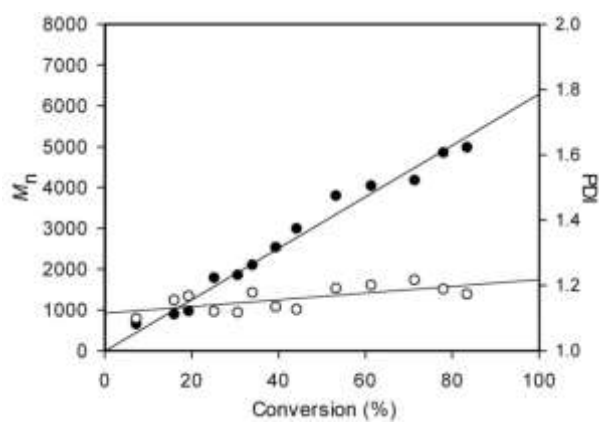


Fig. S23 Plots of PLA M_n (●) and PDI (○) as a function of monomer conversion for a *rac*-LA polymerization using **5b**/PhCH₂OH ([LA]₀/[Al] = 50, toluene, 70 °C)

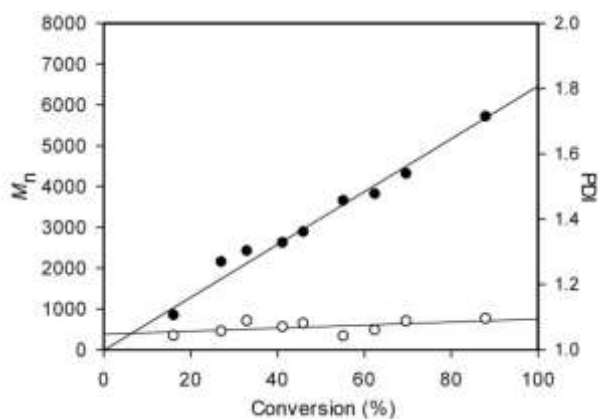


Fig. S24 Plots of PLA M_n (●) and PDI (○) as a function of monomer conversion for a *rac*-LA polymerization using **6a**/PhCH₂OH ([LA]₀/[Al] = 50, toluene, 70 °C)

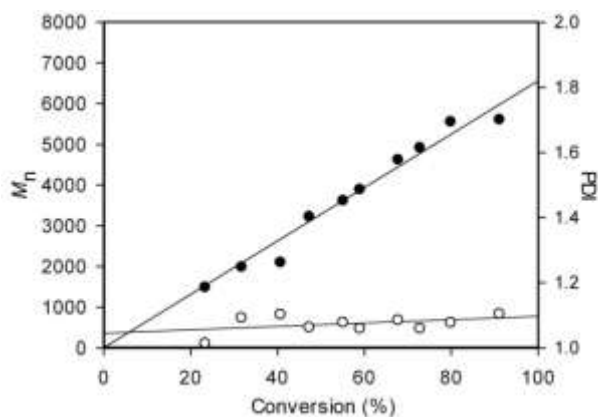


Fig. S25 Plots of PLA M_n (●) and PDI (○) as a function of monomer conversion for a *rac*-LA polymerization using **6b**/PhCH₂OH ([LA]₀/[Al] = 50, toluene, 70 °C)

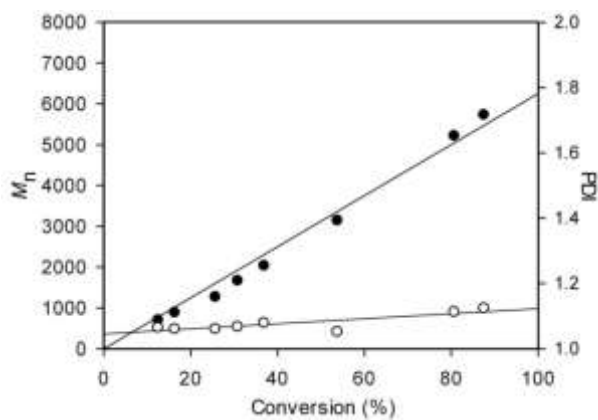


Fig. S26 Plots of PLA M_n (●) and PDI (○) as a function of monomer conversion for a *rac*-LA polymerization using **7a**/PhCH₂OH ([LA]₀/[Al] = 50, toluene, 70 °C)

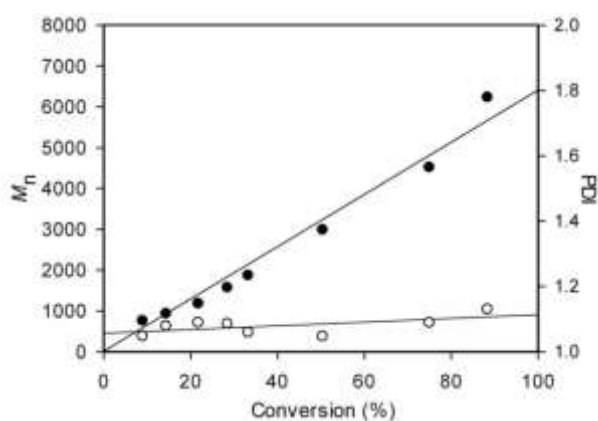


Fig. S27 Plots of PLA M_n (●) and PDI (○) as a function of monomer conversion for a *rac*-LA polymerization using **7b**/PhCH₂OH ([LA]₀/[Al] = 50, toluene, 70 °C)

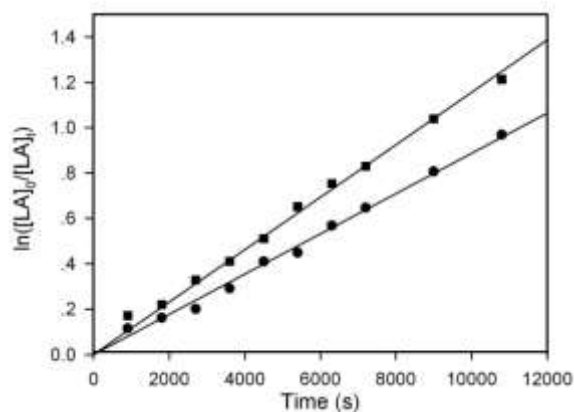


Fig. S28 Semilogarithmic plots of *rac*-lactide conversion *versus* time in toluene at 70 °C with complexes **2a** (●) and **2b** (■) ([LA]₀/[Al] = 50, [Al]/[PhCH₂OH] = 1, [LA]₀ = 0.42 M, [Al] = 8.33 mM).

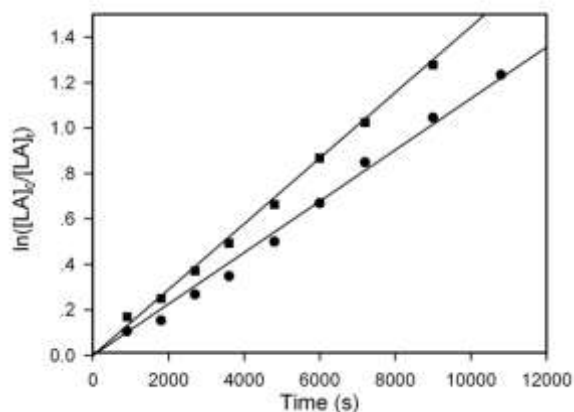


Fig. S29 Semilogarithmic plots of *rac*-lactide conversion *versus* time in toluene at 70 °C with complexes **3a** (●) and **3b** (■) ([LA]₀/[Al] = 50, [Al]/[PhCH₂OH] = 1, [LA]₀ = 0.42 M, [Al] = 8.33 mM).

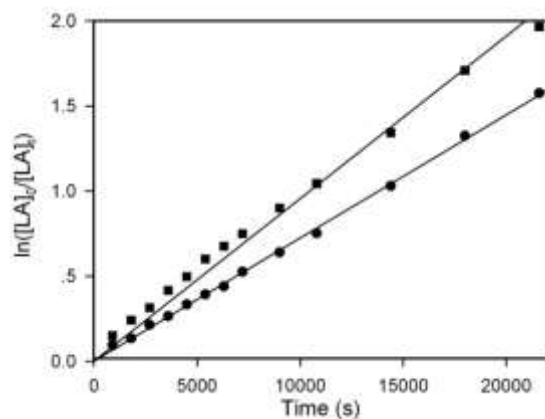


Fig. S30 Semilogarithmic plots of *rac*-lactide conversion *versus* time in toluene at 70 °C with complexes **4a** (●) and **4b** (■) ($[LA]_0/[Al] = 50$, $[Al]/[PhCH_2OH] = 1$, $[LA]_0 = 0.42$ M, $[Al] = 8.33$ mM).

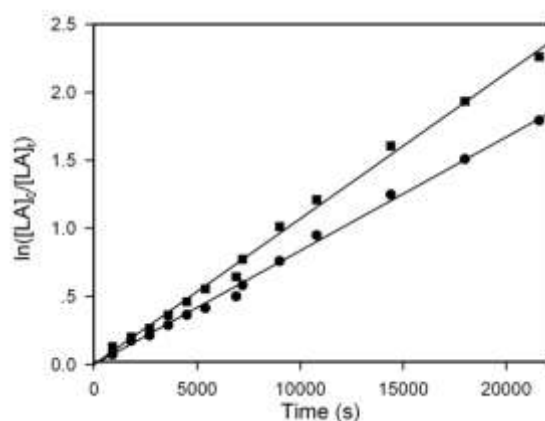


Fig. S31 Semilogarithmic plots of *rac*-lactide conversion *versus* time in toluene at 70 °C with complexes **5a** (●) and **5b** (■) ($[LA]_0/[Al] = 50$, $[Al]/[PhCH_2OH] = 1$, $[LA]_0 = 0.42$ M, $[Al] = 8.33$ mM).

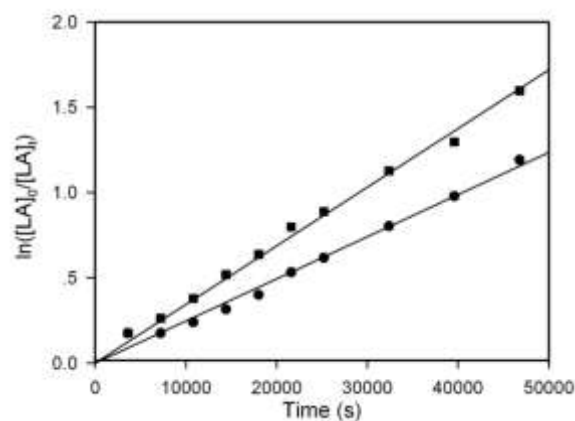


Fig. S32 Semilogarithmic plots of *rac*-lactide conversion *versus* time in toluene at 70 °C with complexes **6a** (●) and **6b** (■) ($[LA]_0/[Al] = 50$, $[Al]/[PhCH_2OH] = 1$, $[LA]_0 = 0.42$ M, $[Al] = 8.33$ mM).

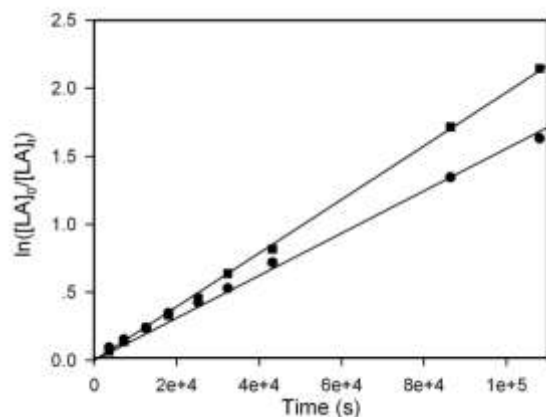


Fig. S33 Semilogarithmic plots of *rac*-lactide conversion *versus* time in toluene at 70 °C with complexes **7a** (●) and **7b** (■) ($[LA]_0/[Al] = 50$, $[Al]/[PhCH_2OH] = 1$, $[LA]_0 = 0.42$ M, $[Al] = 8.33$ mM).

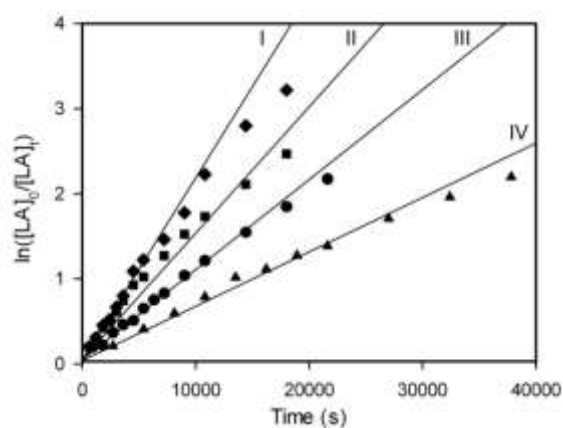


Fig. S34 Semilogarithmic plots of the *rac*-lactide conversion *versus* time in toluene at 70 °C with complex **1b**/ $PhCH_2OH$ as an initiator ($[LA]_0 = 0.42$ M: **I**, $[Al] = 16.65$ mM, $[LA]_0/[Al] = 25$; **II**, $[Al] = 12.49$ mM, $[LA]_0/[Al] = 34$; **III**, $[Al] = 8.33$ mM, $[LA]_0/[Al] = 50$; **IV**, $[Al] = 6.24$ mM, $[LA]_0/[Al] = 67$).

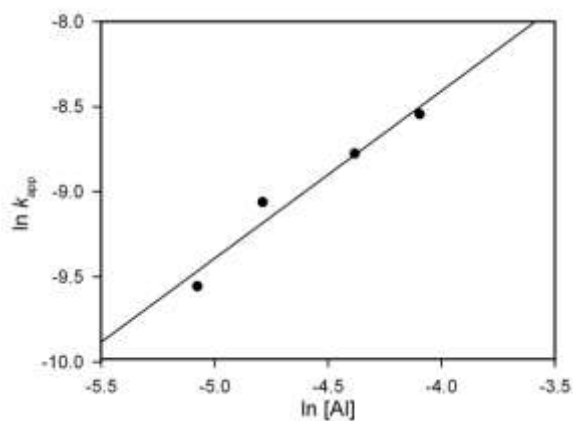


Fig. S35 Plot of $\ln k_{app}$ *versus* $\ln [Al]$ for the polymerization of *rac*-lactide with complex **1b**/ $PhCH_2OH$ as an initiator (toluene, 70 °C, $[LA]_0 = 0.42$ M).

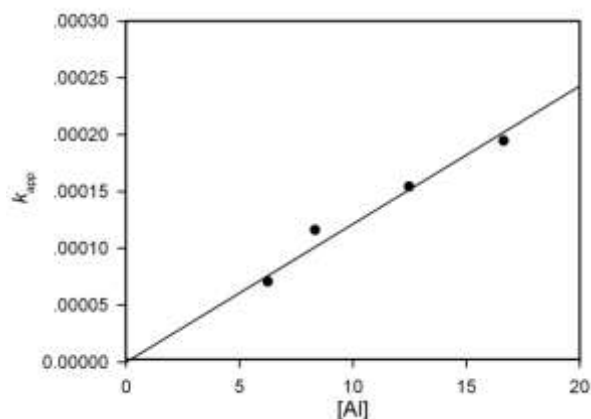


Fig. S36 Plot of k_{app} versus $[Al]$ for the polymerization of *rac*-lactide with complex **1b**/PhCH₂OH as an initiator (toluene, 70 °C, $[LA]_0 = 0.42$ M).

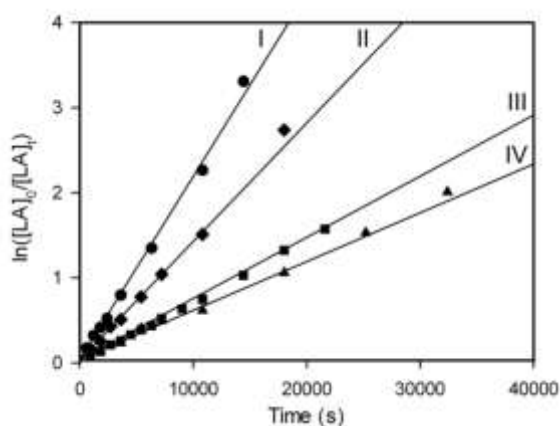


Fig. S37 Semilogarithmic plots of the *rac*-lactide conversion versus time in toluene at 70 °C with complex **4a**/PhCH₂OH as an initiator ($[LA]_0 = 0.42$ M: **I**, $[Al] = 16.65$ mM, $[LA]_0/[Al] = 25$; **II**, $[Al] = 12.49$ mM, $[LA]_0/[Al] = 34$; **III**, $[Al] = 8.33$ mM, $[LA]_0/[Al] = 50$; **IV**, $[Al] = 6.24$ mM, $[LA]_0/[Al] = 67$).

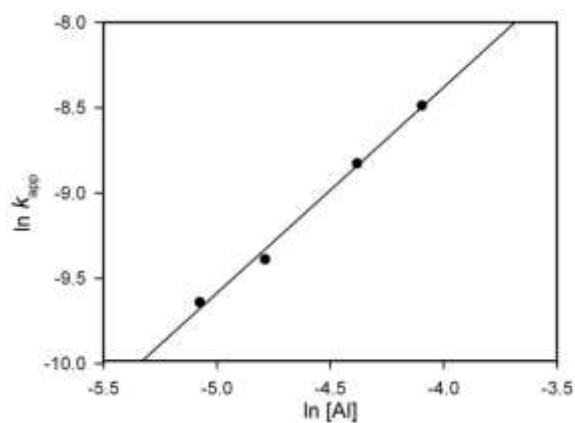


Fig. S38 Plot of $\ln k_{app}$ versus $\ln [Al]$ for the polymerization of *rac*-lactide with complex **4a**/PhCH₂OH as an initiator (toluene, 70 °C, $[LA]_0 = 0.42$ M).

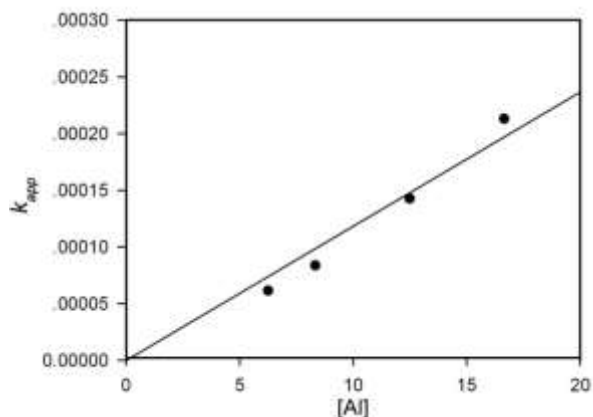


Fig. S39 Plot of k_{app} versus $[A]$ for the polymerization of *rac*-lactide with complex **4a**/PhCH₂OH as an initiator (toluene, 70 °C, $[LA]_0 = 0.42$ M).

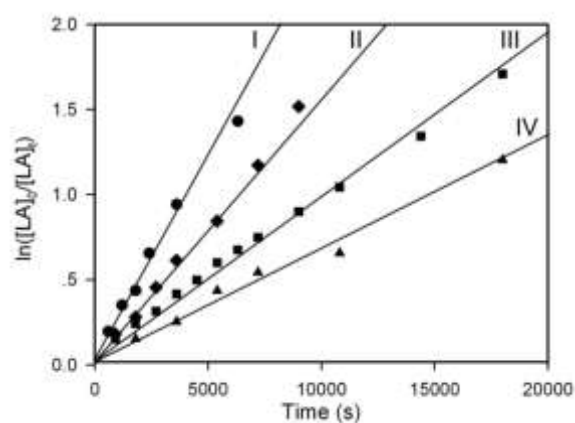


Fig. S40 Semilogarithmic plots of the *rac*-lactide conversion versus time in toluene at 70 °C with complex **4b**/PhCH₂OH as an initiator ($[LA]_0 = 0.42$ M: **I**, $[A] = 16.65$ mM, $[LA]_0/[A] = 25$; **II**, $[A] = 12.49$ mM, $[LA]_0/[A] = 34$; **III**, $[A] = 8.33$ mM, $[LA]_0/[A] = 50$; **IV**, $[A] = 6.24$ mM, $[LA]_0/[A] = 67$).

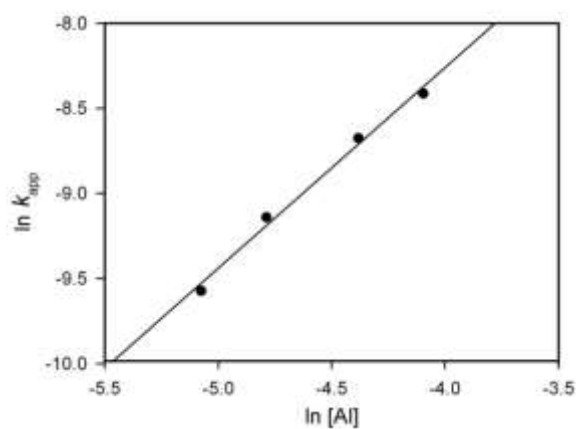


Fig. S41 Plot of $\ln k_{app}$ versus $\ln [A]$ for the polymerization of *rac*-lactide with complex **4b**/PhCH₂OH as an initiator (toluene, 70 °C, $[LA]_0 = 0.42$ M).

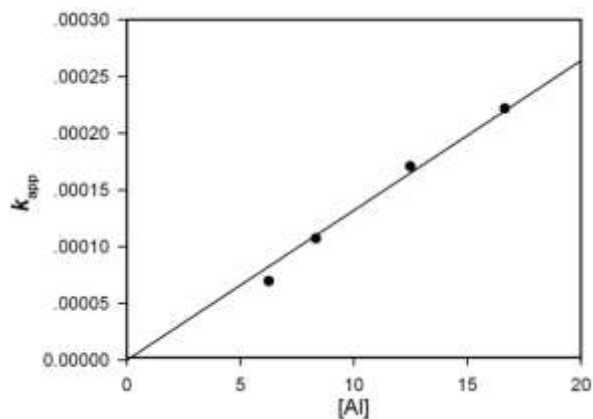


Fig. S42 Plot of k_{app} versus $[A]$ for the polymerization of *rac*-lactide with complex **4b**/PhCH₂OH as an initiator (toluene, 70 °C, $[LA]_0 = 0.42$ M).

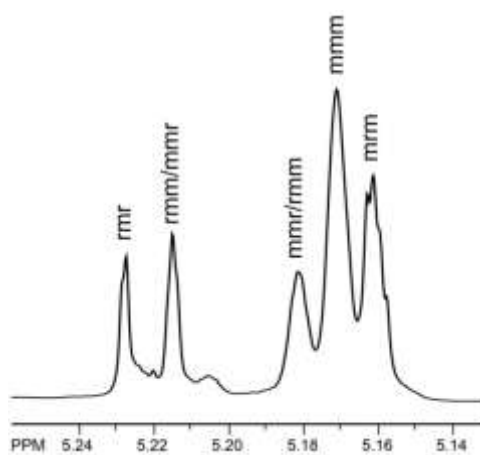


Fig. S43 Homocoupled ¹H NMR spectra of the methine region of PLA prepared from *rac*-lactide with **1a**/PhCH₂OH at 70 °C in toluene (500 MHz, CDCl₃).

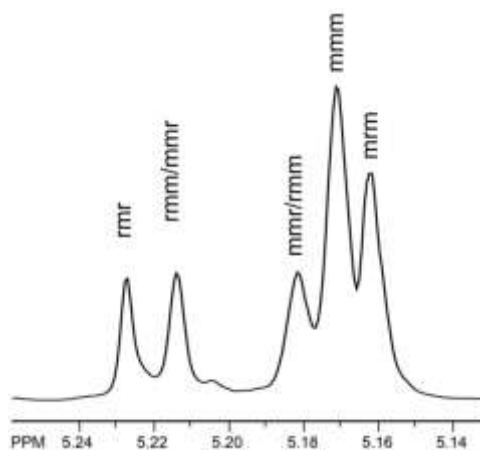


Fig. S44 Homocoupled ¹H NMR spectra of the methine region of PLA prepared from *rac*-lactide with **1b**/PhCH₂OH at 70 °C in toluene (500 MHz, CDCl₃).

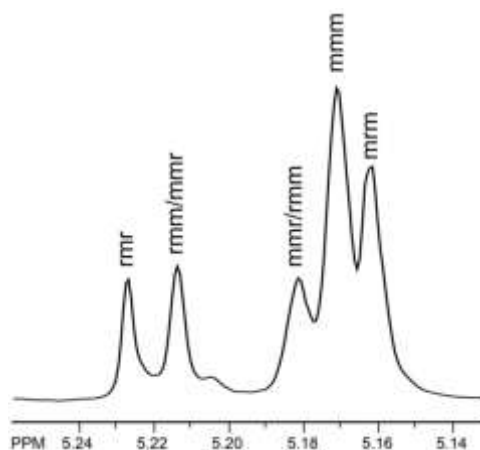


Fig. S45 Homonuclear decoupled ^1H NMR spectra of the methine region of PLA prepared from *rac*-lactide with **2a**/ PhCH_2OH at $70\text{ }^\circ\text{C}$ in toluene (500 MHz, CDCl_3).

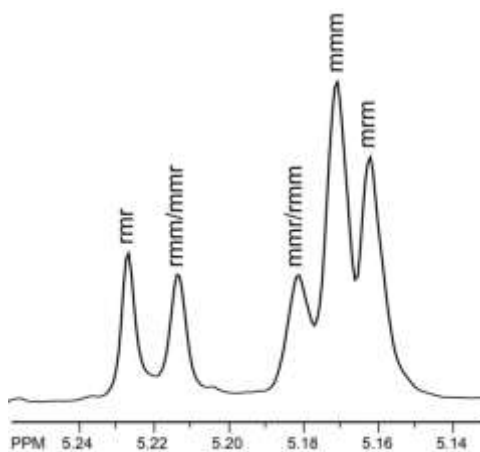


Fig. S46 Homonuclear decoupled ^1H NMR spectra of the methine region of PLA prepared from *rac*-lactide with **2b**/ PhCH_2OH at $70\text{ }^\circ\text{C}$ in toluene (500 MHz, CDCl_3).

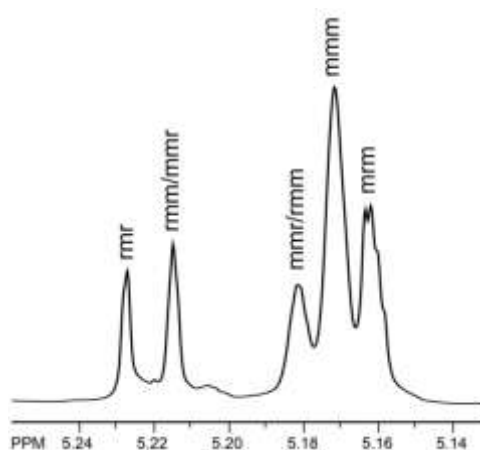


Fig. S47 Homonuclear decoupled ^1H NMR spectra of the methine region of PLA prepared from *rac*-lactide with **3a**/ PhCH_2OH at $70\text{ }^\circ\text{C}$ in toluene (500 MHz, CDCl_3).

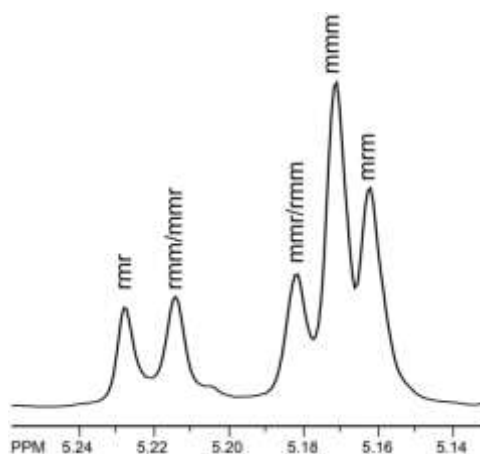


Fig. S48 Homonuclear decoupled ^1H NMR spectra of the methine region of PLA prepared from *rac*-lactide with **3b**/PhCH₂OH at 70 °C in toluene (500 MHz, CDCl₃).

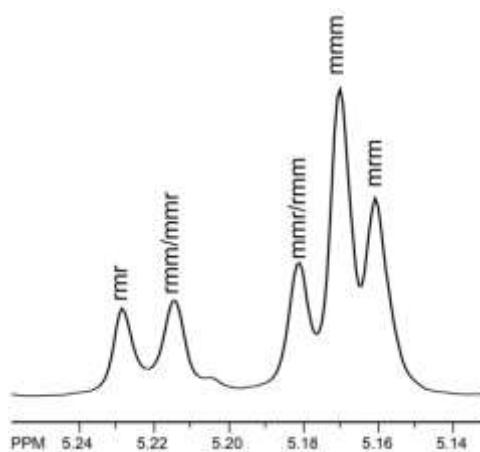


Fig. S49 Homonuclear decoupled ^1H NMR spectra of the methine region of PLA prepared from *rac*-lactide with **4a**/PhCH₂OH at 70 °C in toluene (500 MHz, CDCl₃).

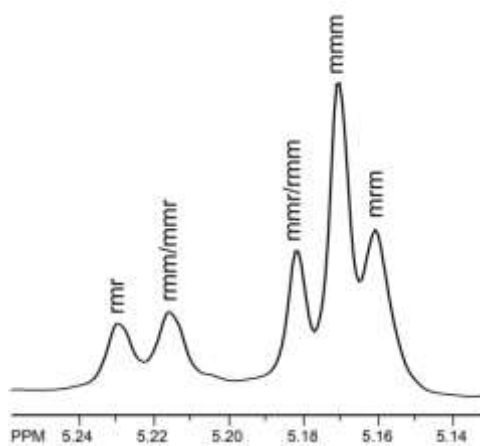


Fig. S50 Homonuclear decoupled ^1H NMR spectra of the methine region of PLA prepared from *rac*-lactide with **4b**/PhCH₂OH at 70 °C in toluene (500 MHz, CDCl₃).

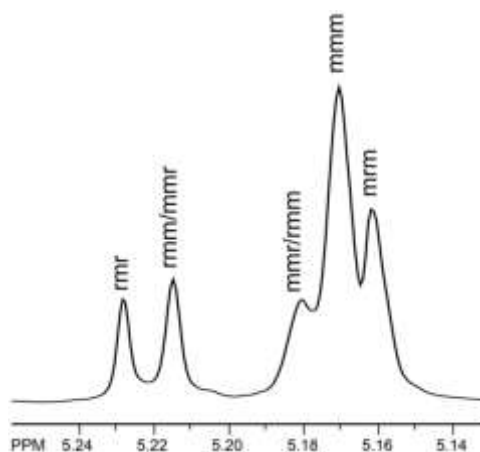


Fig. S51 Homonuclear decoupled ^1H NMR spectra of the methine region of PLA prepared from *rac*-lactide with **5a**/ PhCH_2OH at $70\text{ }^\circ\text{C}$ in toluene (500 MHz, CDCl_3).

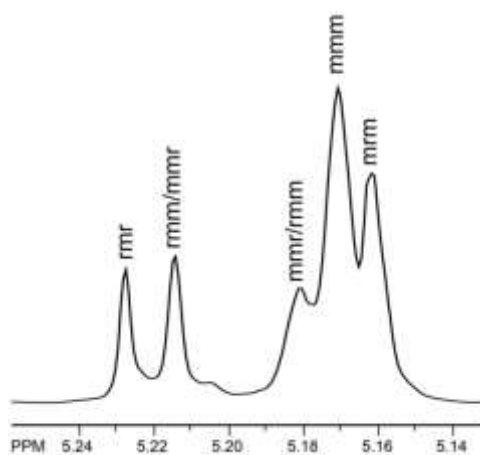


Fig. S52 Homonuclear decoupled ^1H NMR spectra of the methine region of PLA prepared from *rac*-lactide with **5b**/ PhCH_2OH at $70\text{ }^\circ\text{C}$ in toluene (500 MHz, CDCl_3).

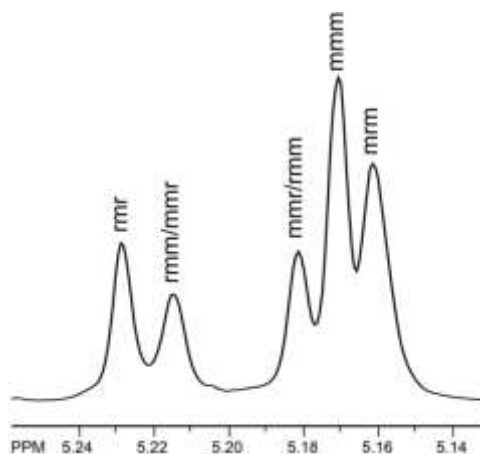


Fig. S53 Homonuclear decoupled ^1H NMR spectra of the methine region of PLA prepared from *rac*-lactide with **6a**/ PhCH_2OH at $70\text{ }^\circ\text{C}$ in toluene (500 MHz, CDCl_3).

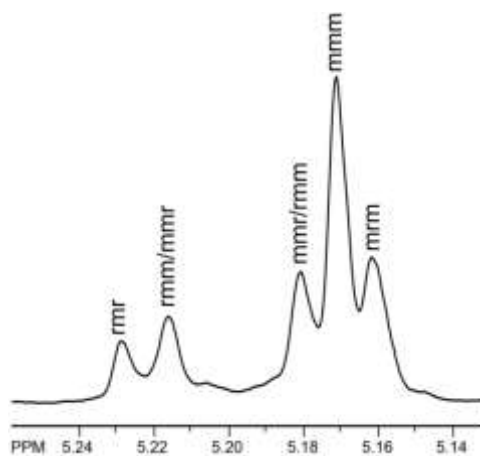


Fig. S54 Homonuclear decoupled ^1H NMR spectra of the methine region of PLA prepared from *rac*-lactide with **7a**/PhCH₂OH at 70 °C in toluene (500 MHz, CDCl₃).